GUARANTEED ERROR CONTROL FOR THE PSEUDOSTRESS APPROXIMATION OF THE STOKES EQUATIONS

P. BRINGMANN, C. CARSTENSEN, AND C. MERDON

Abstract. The pseudostress approximation of the Stokes equations rewrites the stationary Stokes equations with pure (but possibly inhomogeneous) Dirichlet boundary conditions as another (equivalent) mixed scheme based on a stress in $H(\mathrm{div})$ and the velocity in L^2. Any standard mixed finite element function space can be utilized for this mixed formulation, e.g. the Raviart-Thomas discretization which is related to the Crouzeix-Raviart nonconforming finite element scheme in the lowest-order case. The effective and guaranteed a posteriori error control for this nonconforming velocity-oriented discretization can be generalized to the error control of some piecewise quadratic velocity approximation that is related to the discrete pseudostress. The analysis allows for local inf-sup constants which can be chosen in a global partition to improve the estimation. Numerical examples provide strong evidence for an effective and guaranteed error control with very small overestimation factors even for domains with large anisotropy.

1. Introduction

The pseudostress finite element method (PS-FEM) has recently been established in the context of a least-squares finite element method for the Stokes equations [1, 2, 3]. The adaptive mesh-refinement leads to optimal convergence rates [4] for the lowest-order case. This and the principle availability for higher polynomial degrees makes this mixed finite element method highly attractive over the nonconforming P_1 finite element method usually attributed to Crouzeix and Raviart.

The error control for finite element methods in the energy norm with residual-based explicit error estimators typically leads to unknown or large multiplicative reliability constants and is usually uncompetitive over refined methodologies like equilibration error estimators that lead to guaranteed upper bounds, see [5, 6, 7] for recent error estimator competitions. In case of nonconforming finite element schemes, one residual in the error analysis concerns the geometric condition that one variable is a distributional gradient of a Sobolev function and thereby involves the design of a particular test-function v near to the discrete solution u_h. For the Stokes problem, the side conditions on this Sobolev function require the match of the true Dirichlet boundary conditions as well as the incompressibility condition $\mathrm{div}\, v = 0$ a.e. in the domain Ω. The relaxation of this later condition has been suggested in [8] based on some regular split of a gradient into a gradient of a divergence-free H^1 function and an L^2-orthogonal remainder. This leads to the guaranteed upper bound of the energy error

$$\left|\!\left|\!\left| u - u_h \right|\!\right|\!\right|_{\mathrm{NC}}^2 \leqslant \eta^2 + \left(\left|\!\left|\!\left| v - u_h \right|\!\right|\!\right|_{\mathrm{NC}} + \left\| \mathrm{div}\, v \right\|_{L^2(\Omega)} / c_0 \right)^2 .$$

The first quantity η depends only on the right-hand side f, while the second term on the right-hand side depends on v. Another advantage of the PS-FEM is the appearance of

2010 *Mathematics Subject Classification.* 65N30,65N15,76D07.

Key words and phrases. nonconforming finite element method, Crouzeix-Raviart element, Stokes equations, pseudostress finite element method, adaptive finite element method, a posteriori error estimation.

This work was supported by DFG Research Center MATHEON and the BMS in Berlin, Germany.

the oscillation of the right-hand side f in η compared to the L^2-norm of the mesh-size times f in the nonconforming case [9]. The stability constant c_0 is an inf-sup constant and difficult to compute, see [10] and [11] for the corrected results. Moreover, c_0 deteriorates for stretched domains with large aspect ratios [12] and so may crucially worsen the efficiency indices of all error estimators based on designs of non divergence-free test-functions. Several such designs were proposed and compared in [8, 13, 14] and mainly stem from popular conforming postprocessings of nonconforming finite element solutions for the Poisson problem [15, 16, 17, 7].

The only approach to compute guaranteed error bounds for the backward facing step from Subsection 5.4 follows the localization technique [9] with a partition $\Omega_1, \dots, \Omega_J$ of Ω and inf-sup constants c_j of Ω_j. When the designed test-function satisfies the additional condition

$$\int_{\partial\Omega_j} v \cdot \nu_{\Omega_j} \,\mathrm{d}s = 0 \quad \text{for } j = 1, \dots, J,$$

the guaranteed upper bound only includes the local inf-sup constants of the subdomains Ω_j, i.e.,

$$|||u - u_h|||_{\mathrm{NC}}^2 \leqslant \eta^2 + \sum_{j=1}^{J} \left(\left\| \mathrm{D}_{\mathrm{NC}}(v - u_h) \right\|_{L^2(\Omega_j)} + \left\| \operatorname{div} v \right\|_{L^2(\Omega_j)} / c_j \right)^2.$$

To mention just two prominent situations, one may think of a decomposition of an L-shaped domain or a long thin channel into squares. Several strategies of how to satisfy the additional constraint within the test-function designs from [13] are discussed in Section 4 below.

The resulting error estimators are studied for the lowest-order PS-FEM where $u_h := u_2$ is some piecewise quadratic function whose piecewise gradient equals the Raviart-Thomas best-approximation of the exact pseudostress [4, 18] up to some pressure contribution. The proposed error estimator designs of the present paper lead to the sharpest guaranteed upper error bounds known for this scheme, even in the case of challenging domains with very small inf-sup constants.

The remaining parts of this paper are organized as follows. Section 2 recalls the Stokes equations and describes the nonconforming finite element discretization. Section 3 presents the pseudostress approximation and states the main result for the guaranteed upper error bound in Theorem 3.1 on page 5. Section 4 designs different interpolations of the discrete velocity which lead to guaranteed upper error bounds. It includes the treatment of inhomogeneous Dirichlet boundary conditions. Finally, Section 5 presents numerical experiments on some benchmark problems.

Standard notation on Lebesgue and Sobolev spaces applies throughout this paper such as $H^k(\Omega)$, $H(\operatorname{div}, \Omega)$, and $L^2(\Omega)$ and the associated spaces for vector- or matrix-valued functions $H^k(\Omega; \mathbb{R}^2)$, $L^2(\Omega; \mathbb{R}^2)$, $H^k(\Omega; \mathbb{R}^{2\times 2})$, $H(\operatorname{div}, \Omega; \mathbb{R}^{2\times 2})$, and $L^2(\Omega; \mathbb{R}^{2\times 2})$. Let $H^1_0(\Omega) := \{v \in H^1(\Omega) : v \equiv 0 \text{ on } \partial\Omega \text{ in the sense of traces}\}$ be equipped with the energy norm

$$|||\cdot||| := |\cdot|_{H^1(\Omega)} = \left\| \mathrm{D} \cdot \right\|_{L^2(\Omega)}.$$

The 2D rotation operators read, for $v \in H^1(\Omega; \mathbb{R}^2)$,

$$\operatorname{Curl} v := \begin{pmatrix} -\partial v_1/\partial x_2 & \partial v_1/\partial x_1 \\ -\partial v_2/\partial x_2 & \partial v_2/\partial x_1 \end{pmatrix} \quad \text{and} \quad \operatorname{curl} v := \operatorname{tr} \operatorname{Curl} v.$$

The expression $A \lesssim B$ abbreviates the relation $A \leqslant CB$ with a generic constant $0 < C$ which solely depends on the interior angles $\sphericalangle\mathcal{T}$ of the underlying triangulation; $A \approx B$ abbreviates $A \lesssim B \lesssim A$.

2. Notation and Preliminaries

2.1. **Stokes equations.** This paper concerns the 2D Stokes equations: Given a right-hand side $f \in L^2(\Omega;\mathbb{R}^2)$ and Dirichlet boundary data $u_D \in H^1(\Omega;\mathbb{R}^2)$ with $\int_{\partial\Omega} u_D \cdot \nu \,\mathrm{d}s = 0$, seek a pressure $p \in L^2_0(\Omega;\mathbb{R}^2) := \{q \in L^2(\Omega;\mathbb{R}^2) : \int_\Omega q \,\mathrm{d}x = 0\}$ and a velocity field $u \in H^1(\Omega;\mathbb{R}^2)$ with

$$-\Delta u + \nabla p = f \quad \text{and} \quad \operatorname{div} u = 0 \text{ in } \Omega \quad \text{while} \quad u = u_D \text{ on } \partial\Omega.$$

The error analysis involves (lower bounds of) the inf-sup constant

$$0 < c_0 := \inf_{q\in L^2_0(\Omega)\setminus\{0\}} \sup_{v\in H^1_0(\Omega;\mathbb{R}^2)\setminus\{0\}} \int_\Omega q \operatorname{div} v \,\mathrm{d}x \Big/ \big(\|\mathrm{D}\, v\|_{L^2(\Omega)} \|q\|_{L^2(\Omega)}\big)$$

that arises in the Ladyzhenskaya lemma [19, §6. Theorem 6.3] and depends on Ω. Lower bounds for this constant are in general difficult to compute, see [10] and for corrected results [11]. Moreover, c_0 gets smaller for stretched domains with large anisotropy [12]. How to circumvent these problems for the error analysis is explained in Section 3 based on [9].

2.2. **Nonconforming finite element spaces.** Given a regular triangulation $\mathcal{T}$ of the bounded Lipschitz domain $\Omega \subseteq \mathbb{R}^2$ into closed triangles in the sense of Ciarlet with the set of edges $\mathcal{E}$, the set of nodes $\mathcal{N}$, the set of interior edges $\mathcal{E}(\Omega)$, the set of interior nodes $\mathcal{N}(\Omega)$, the set $\mathcal{E}(\partial\Omega)$ of edges along the boundary $\partial\Omega$ and the set of boundary nodes $\mathcal{N}(\partial\Omega)$, define the set $\operatorname{mid}(\mathcal{E}) := \{\operatorname{mid}(E) : E \in \mathcal{E}\}$ of midpoints of all edges and let $\mathcal{E}(T)$ be the set of the three edges and let $\mathcal{N}(T)$ be the set of the three vertices of a triangle $T \in \mathcal{T}$. Let the set $\mathcal{T}(z)$ contain all triangles $T \in \mathcal{T}$ with vertex $z \in \mathcal{N}(T)$ for a node $z \in \mathcal{N}$ and denote its cardinality with $\big|\mathcal{T}(z)\big|$. The diameter $\operatorname{diam}(T)$ of $T \in \mathcal{T}$ is denoted by h_T and $h_{\mathcal{T}}$ denotes their piecewise constant values with $h_{\mathcal{T}}|_T := h_T := \operatorname{diam}(T)$ for all $T \in \mathcal{T}$. With the elementwise polynomials $P_k(\mathcal{T};\mathbb{R}^2)$ of degree at most k, the nonconforming Crouzeix-Raviart finite element spaces read

$$\mathrm{CR}^1(\mathcal{T};\mathbb{R}^2) := \{v \in P_1(\mathcal{T};\mathbb{R}^2) : \forall E \in \mathcal{E},\ v \text{ is continuous at } \operatorname{mid}(E)\},$$
$$\mathrm{CR}^1_0(\mathcal{T};\mathbb{R}^2) := \{v \in \mathrm{CR}^1(\mathcal{T};\mathbb{R}^2) : \forall E \in \mathcal{E}(\partial\Omega),\ v(\operatorname{mid}(E)) = 0\}.$$

The Crouzeix-Raviart finite element functions form a subspace of the piecewise Sobolev functions

$$H^1(\mathcal{T}) := \{v \in L^2(\Omega) : \forall T \in \mathcal{T},\, v|_T \in H^1(T) := H^1(\operatorname{int}(T))\}$$

with corresponding piecewise differential operators D_{NC} and $\operatorname{div}_{\mathrm{NC}}$.

The integral mean of a function $f \in L^2(\omega)$ (or any vector $f \in L^2(\omega;\mathbb{R}^2)$) over some open set ω is denoted by

$$f_\omega := \fint_\omega f \,\mathrm{d}x := \int_\omega f \,\mathrm{d}x \Big/ |\omega|.$$

The oscillations of $f \in L^2(\Omega)$ (as well as of vectors $f \in L^2(\Omega;\mathbb{R}^2)$) read

$$\operatorname{osc}^2(f,\mathcal{T}) := \sum_{T\in\mathcal{T}} \operatorname{osc}^2(f,T) = \big\|h_{\mathcal{T}}(f - f_{\mathcal{T}})\big\|^2_{L^2(\Omega)} \quad \text{with} \quad \operatorname{osc}^2(f,\mathcal{T}) := \big\|h_T(f - f_T)\big\|^2_{L^2(T)},$$

where $f_{\mathcal{T}} := \Pi f$ denotes the L^2-orthogonal projection of f onto the piecewise constant functions $P_0(\mathcal{T})$ (respectively $P_0(\mathcal{T};\mathbb{R}^2)$).

Finally, define the right-hand side functional for given $f \in L^2(\Omega;\mathbb{R}^2)$ by

$$F(v) := \int_\Omega f \cdot v \,\mathrm{d}x \quad \text{for all } v \in H^1(\mathcal{T};\mathbb{R}^2). \tag{2.1}$$

2.3. **Crouzeix-Raviart FEM for the Stokes equations.** The first discrete bilinear form reads

$$a_{\mathrm{NC}}(u_{\mathrm{CR}}, v_{\mathrm{CR}}) \coloneqq \sum_{T\in\mathcal{T}} \int_T \mathrm{D}\, u_{\mathrm{CR}} : \mathrm{D}\, v_{\mathrm{CR}}\, \mathrm{d}x$$

for all $u_{\mathrm{CR}}, v_{\mathrm{CR}} \in \mathrm{CR}^1(\mathcal{T};\mathbb{R}^2) \subseteq H^1(\mathcal{T};\mathbb{R}^2)$ with $A : B \coloneqq \sum_{j,k=1,2} A_{jk}B_{jk}$ for all 2×2 matrices $A, B \in \mathbb{R}^{2\times 2}$. Let $L^2_0(\Omega) \coloneqq \{q \in L^2(\Omega) : \int_\Omega q\,\mathrm{d}x = 0\}$ denote the space of L^2 functions with zero integral mean. Then, the second discrete bilinear form reads

$$b_{\mathrm{NC}}(v_{\mathrm{CR}}, q_0) \coloneqq \int_\Omega q_0 \,\mathrm{div}_{\mathrm{NC}}\, v_{\mathrm{CR}}\, \mathrm{d}x$$

for all $v_{\mathrm{CR}} \in \mathrm{CR}^1_0(\mathcal{T};\mathbb{R}^2)$ and $q_0 \in P_0(\mathcal{T}) \cap L^2_0(\Omega)$. This leads to the discrete counterpart

$$Z_{\mathrm{NC}} \coloneqq \{v_{\mathrm{CR}} \in \mathrm{CR}^1_0(\mathcal{T};\mathbb{R}^2) : \mathrm{div}_{\mathrm{NC}}\, v_{\mathrm{CR}} = 0 \text{ a.e. in } \Omega\}$$

of the set of divergence-free functions

$$Z \coloneqq \{v \in H^1_0(\Omega;\mathbb{R}^2) : \mathrm{div}\, v = 0 \text{ a.e. in } \Omega\}.$$

The nonconforming representation of the Stokes problem reads: Given $f \in L^2(\Omega;\mathbb{R}^2)$ and $u_D \in L^2(\Omega;\mathbb{R}^2)$ with $\int_{\partial\Omega} u_D \cdot \nu\,\mathrm{d}s = 0$, seek $u_{\mathrm{CR}} \in Z_{\mathrm{NC}}$ with

$$u_{\mathrm{CR}}(\mathrm{mid}(E)) = \fint_E u_D\,\mathrm{d}s \quad \text{for all } E \in \mathcal{E}(\partial\Omega)$$

and

$$a_{\mathrm{NC}}(u_{\mathrm{CR}}, v_{\mathrm{CR}}) = F(v_{\mathrm{CR}}) \quad \text{for all } v_{\mathrm{CR}} \in Z_{\mathrm{NC}}.$$

In other words, up to boundary conditions, u_{CR} is computed from the Riesz representation of a linear functional (given as right-hand side plus boundary modifications) in the Hilbert space $(Z_{\mathrm{NC}}, a_{\mathrm{NC}})$. The actual implementation uses unconstrained Crouzeix-Raviart elements $v_{\mathrm{CR}} \in \mathrm{CR}^1_0(\mathcal{T};\mathbb{R}^2)$ as test functions and enforce the constraint $\mathrm{div}_{\mathrm{NC}}\, u_{\mathrm{CR}} = 0$ a.e. in Ω by piecewise constant Lagrange multipliers in $P_0(\mathcal{T}) \cap L^2_0(\Omega)$. Hence, u_{CR} from above and some $p_{\mathrm{CR}} \in P_0(\mathcal{T}) \cap L^2_0(\Omega)$ are determined by

$$\begin{aligned} a_{\mathrm{NC}}(u_{\mathrm{CR}}, v_{\mathrm{CR}}) + b_{\mathrm{NC}}(v_{\mathrm{CR}}, p_{\mathrm{CR}}) &= F(v_{\mathrm{CR}}) && \text{for all } v_{\mathrm{CR}} \in \mathrm{CR}^1_0(\mathcal{T};\mathbb{R}^2),\\ b_{\mathrm{NC}}(u_{\mathrm{CR}}, q_{\mathrm{CR}}) &= 0 && \text{for all } q_{\mathrm{CR}} \in P_0(\mathcal{T}) \cap L^2_0(\Omega). \end{aligned}$$

3. Pseudostress Approximation and Error Analysis

A simple postprocessing of the Crouzeix-Raviart nonconforming solution $\widehat{u}_{\mathrm{CR}} \in Z_{\mathrm{NC}}$ and $\widehat{p}_{\mathrm{CR}} \in P_0(\mathcal{T}) \cap L^2_0(\Omega)$ for the piecewise constant right-hand side $f_{\mathcal{T}}$ (instead of f in (2.1)) leads to the pseudostress representation

$$\begin{aligned} \sigma_{\mathrm{PS}} &\coloneqq \mathrm{D}_{\mathrm{NC}}\, \widehat{u}_{\mathrm{CR}} - \frac{f_{\mathcal{T}}}{2} \otimes (\bullet - \mathrm{mid}(\mathcal{T})) - \widehat{p}_{\mathrm{CR}} I_{2\times 2} \quad \text{and}\\ u_{\mathrm{PS}} &\coloneqq \Pi\widehat{u}_{\mathrm{CR}} + \frac{1}{4}\Pi(\mathrm{dev}(f_{\mathcal{T}} \otimes (\bullet - \mathrm{mid}(\mathcal{T})))(\bullet - \mathrm{mid}(\mathcal{T}))), \end{aligned}$$

where $\mathrm{mid}(\mathcal{T})$ denotes the piecewise constant vector-valued function with $\mathrm{mid}(\mathcal{T})|_T := \mathrm{mid}(T)$ and $\mathrm{dev}(A) := A - \mathrm{tr}(A)\, I_{2\times 2}/2$ denotes the deviatoric part of some matrix-valued function A. Then, the piecewise quadratic function

$$u_2 \coloneqq \widehat{u}_{\mathrm{CR}} - \frac{f_{\mathcal{T}}}{4}\left(\left|\bullet - \mathrm{mid}(\mathcal{T})\right|^2 - \left\|\bullet - \mathrm{mid}(\mathcal{T})\right\|^2_{L^2(\Omega)}\right) \in P_2(\mathcal{T};\mathbb{R}^2)$$

satisfies $\mathrm{D}_{\mathrm{NC}}\, u_2 = \sigma_{\mathrm{PS}} + \widehat{p}_{\mathrm{CR}} I_{2\times 2}$.

The pair $(\sigma_{\rm PS}, u_{\rm PS})$ solves the Raviart-Thomas mixed FEM [4, 3] to approximate the exact pseudostress

$$\sigma := Du - pI_{2\times 2} \in H(\mathrm{div},\Omega;\mathbb{R}^{2\times 2})/\mathbb{R} := \left\{\tau \in H(\mathrm{div},\Omega;\mathbb{R}^{2\times 2}) \,:\, \int_\Omega \mathrm{tr}\,\tau\,\mathrm{d}x = 0\right\}$$

with $f + \mathrm{div}\,\sigma = 0$ and the exact solution $u \in H^1(\Omega;\mathbb{R}^2)$ in the discrete spaces

$$\mathrm{PS}(\mathcal{T}) := \left\{\tau \in P_1(\mathcal{T};\mathbb{R}^{2\times 2}) \cap H(\mathrm{div},\Omega;\mathbb{R}^{2\times 2})/\mathbb{R} \,:\, \forall j = 1,2, (\tau_{j1},\tau_{j2}) \in \mathrm{RT}_0(\mathcal{T})\right\}$$

and $P_0(\mathcal{T};\mathbb{R}^2)$ such that $\mathrm{div}\,\sigma_{\rm PS} + f_{\mathcal{T}} = 0$ a.e. in Ω. In fact, the following discrete formulation has the unique solution $(\sigma_{\rm PS}, u_{\rm PS}) \in \mathrm{PS}(\mathcal{T}) \times P_0(\mathcal{T};\mathbb{R}^2)$,

$$\int_\Omega \mathrm{dev}\,\sigma_{\rm PS} : \tau_{\rm PS}\,\mathrm{d}x + \int_\Omega \mathrm{div}\,\tau_{\rm PS}\cdot u_{\rm PS}\,\mathrm{d}x = \int_{\partial\Omega} u_D\cdot\tau_{\rm PS}\nu\,\mathrm{d}s \quad \text{for all } \tau_{\rm PS}\in \mathrm{PS}(\mathcal{T}), \tag{3.1}$$

$$\int_\Omega \mathrm{div}\,\sigma_{\rm PS}\cdot v_{\rm PS}\,\mathrm{d}x = -\int_\Omega f\cdot v_{\rm PS}\,\mathrm{d}x \quad \text{for all } v_{\rm PS}\in P_0(\mathcal{T};\mathbb{R}^2). \tag{3.2}$$

The following theorem recovers the known results for the Crouzeix-Raviart finite element method from [13, 8] for the pseudostress-related approximation u_2 with the set of admissible test functions $\mathcal{A} := \{v \in H^1(\Omega;\mathbb{R}^2) \,:\, v = u_D \text{ on } \partial\Omega\}$. Moreover, a refined guaranteed upper bound that follows an idea from [9] is introduced. This idea is based on a partition of Ω into J many subdomains $\Omega_1,\dots,\Omega_J$ with $\bigcup_{j=1}^J \overline{\Omega_j} = \overline{\Omega}$, outer unit normal vectors ν_{Ω_j} and local inf-sup constants

$$0 < c_j := \inf_{q\in L^2_0(\Omega_j)\setminus\{0\}} \sup_{v\in H^1_0(\Omega_j;\mathbb{R}^2)\setminus\{0\}} \int_{\Omega_j} q\,\mathrm{div}\,v\,\mathrm{d}x \Big/ \left(\|\,\mathrm{D}\,v\|_{L^2(\Omega_j)}\|q\|_{L^2(\Omega_j)}\right) \quad \text{for } j = 1,\dots,J.$$

The set of test functions that are suitable for the refined error control satisfy an additional contraint and are defined by

$$\widetilde{\mathcal{A}} := \left\{v\in\mathcal{A} \,:\, \int_{\partial\Omega_j} v\cdot\nu_{\Omega_j}\,\mathrm{d}s = 0 \quad \text{for } j = 1,\dots,J\right\}. \tag{3.3}$$

Moreover, the constant $j_{1,1} \geqslant 3.8317$ below denotes the first positive root of the first Bessel function.

Theorem 3.1. *(a) Any $v \in \mathcal{A}$ satisfies*

$$\|\!|u - u_2|\!|^2_{\rm NC} \leqslant \mathrm{osc}(f,\mathcal{T})^2/j_{1,1}^2 + \left(\|\!|v-u_2|\!|_{\rm NC} + \|\,\mathrm{div}\,v\|_{L^2(\Omega)}/c_0\right)^2.$$

(b) Any $v \in \widetilde{\mathcal{A}}$ from (3.3) *satisfies*

$$\|\!|u - u_2|\!|^2_{\rm NC} \leqslant \mathrm{osc}(f,\mathcal{T})^2/j_{1,1}^2 + \sum_{j=1}^J \left(\|\,\mathrm{D_{NC}}(v-u_2)\|_{L^2(\Omega_j)} + \|\,\mathrm{div}\,v\|_{L^2(\Omega_j)}/c_j\right)^2.$$

Proof of Theorem 3.1 (a). The point of departure is the orthogonal split from [8, Subsection 3.2],

$$\mathrm{D_{NC}}(u-u_2) = \mathrm{D}\,z + y \tag{3.4}$$

into some $z \in Z$ with

$$\int_\Omega \mathrm{D}\,z : \mathrm{D}\,v\,\mathrm{d}x = \int_\Omega \mathrm{D_{NC}}(u-u_2) : \mathrm{D}\,v\,\mathrm{d}x \quad \text{for all } v\in Z$$

and the remainder

$$y \in Y := \left\{y\in L^2(\Omega;\mathbb{R}^{2\times 2}) \,:\, \int_\Omega y : \mathrm{D}\,v\,\mathrm{d}x = 0 \text{ for all } v\in Z\right\}.$$

Since Y is the orthogonal complement of $\mathrm{D}(Z)$ in $L^2(\Omega;\mathbb{R}^{2\times 2})$, it follows

$$\|\!|u-u_2|\!\|_{\mathrm{NC}}^2 = \|\!|z|\!\|^2 + \|y\|_{L^2(\Omega)}^2. \tag{3.5}$$

Since $z\in Z$, $I_{2\times 2}:\mathrm{D}\,z=\operatorname{div} z=0$ a.e. This, the aforementioned orthogonality, and an integration by parts show

$$\begin{aligned}\|\!|z|\!\|^2 &= \int_\Omega \mathrm{D}_{\mathrm{NC}}(u-u_2):\mathrm{D}\,z\,\mathrm{d}x = \int_\Omega \mathrm{D}\,u:\mathrm{D}\,z\,\mathrm{d}x - \int_\Omega \mathrm{D}_{\mathrm{NC}}\,u_2:\mathrm{D}\,z\,\mathrm{d}x\\ &= \int_\Omega f\cdot z\,\mathrm{d}x - \int_\Omega \sigma_{\mathrm{PS}}:\mathrm{D}\,z\,\mathrm{d}x = \int_\Omega f\cdot z\,\mathrm{d}x + \int_\Omega z\cdot\operatorname{div}\sigma_{\mathrm{PS}}\,\mathrm{d}x = \int_\Omega (f-f_{\mathcal{T}})\cdot z\,\mathrm{d}x.\end{aligned}$$

Piecewise Poincaré inequalities (with Poincaré constant $h_T/j_{1,1}$ from [20, Corollary 3.4]) then imply

$$\begin{aligned}\int_\Omega (f-f_{\mathcal{T}})\cdot z\,\mathrm{d}x &= \int_\Omega (f-f_{\mathcal{T}})\cdot(z-z_{\mathcal{T}})\,\mathrm{d}x \leqslant \sum_{T\in\mathcal{T}} \|f-f_T\|_{L^2(T)}\|z-z_T\|_{L^2(T)}\\ &\leqslant \sum_{T\in\mathcal{T}} h_T/j_{1,1}\,\|f-f_T\|_{L^2(T)}\|\,\mathrm{D}\,z\|_{L^2(T)} \leqslant \operatorname{osc}(f,\mathcal{T})/j_{1,1}\,\|\!|z|\!\|.\end{aligned}$$

Hence,

$$\|\!|z|\!\| \leqslant \operatorname{osc}(f,\mathcal{T})/j_{1,1}. \tag{3.6}$$

Recall from [8, Subsection 3.2, Lemma 2] that, for each $y\in Y$, there exists some $q\in L^2_0(\Omega)$ with

$$\int_\Omega y:\mathrm{D}\,w\,\mathrm{d}x = \int_\Omega q\operatorname{div} w\,\mathrm{d}x \quad \text{for all } w\in H^1_0(\Omega;\mathbb{R}^2)$$

and

$$c_0\|q\|_{L^2(\Omega)} \leqslant \|y\|_{L^2(\Omega)}.$$

Hence, any $v\in\mathcal{A}$ with $u-v=0$ on $\partial\Omega$ satisfies

$$\begin{aligned}\|y\|_{L^2(\Omega)}^2 &= \int_\Omega \mathrm{D}_{\mathrm{NC}}(u-u_2):y\,\mathrm{d}x = \int_\Omega \mathrm{D}_{\mathrm{NC}}(v-u_2):y\,\mathrm{d}x + \int_\Omega \mathrm{D}(u-v):y\,\mathrm{d}x\\ &= \int_\Omega \mathrm{D}_{\mathrm{NC}}(v-u_2):y\,\mathrm{d}x + \int_\Omega q\operatorname{div}(u-v)\,\mathrm{d}x\\ &\leqslant \Big(\|\,\mathrm{D}_{\mathrm{NC}}(v-u_2)\|_{L^2(\Omega)} + \|\operatorname{div} v\|_{L^2(\Omega)}/c_0\Big)\,\|y\|_{L^2(\Omega)}.\end{aligned}$$

Therefore,

$$\|y\|_{L^2(\Omega)} \leqslant \|\,\mathrm{D}_{\mathrm{NC}}(v-u_2)\|_{L^2(\Omega)} + \|\operatorname{div}(v)\|_{L^2(\Omega)}/c_0. \tag{3.7}$$

The combination of (3.5)–(3.7) concludes the proof. □

Proof of Theorem 3.1 (b). The proof follows ideas from [9] for the local versions

$$\begin{aligned}Z_j &:= \{z\in H^1_0(\Omega_j;\mathbb{R}^2) \,:\, \operatorname{div} z=0 \text{ a.e. in } \Omega_j\} \quad \text{and}\\ Y_j &:= \Big\{y\in L^2(\Omega_j;\mathbb{R}^{2\times 2}) \,:\, \int_{\Omega_j} y:\mathrm{D}\,z\,\mathrm{d}x = 0 \text{ for all } z\in Z_j\Big\}\end{aligned}$$

of Z and Y from the proof of (a) with Ω replaced by Ω_j.

Given $v\in\widetilde{\mathcal{A}}$ and any $j=1,\dots,J$, the condition

$$\int_{\partial\Omega_j} v\cdot\nu_j ds = 0$$

guarantees that the Stokes equations with volume force $f_{\mathcal{T}}$ has a unique solution $w_j \in Z_j$ with the boundary data $w_j = v$ along $\partial\Omega_j$, i.e.,

$$\int_{\Omega_j} \mathrm{D}\, w_j : \mathrm{D}\, \zeta_j \,\mathrm{d}x = \int_{\Omega_j} f_{\mathcal{T}} \cdot \zeta_j \,\mathrm{d}x \quad \text{for all } \zeta_j \in Z_j. \tag{3.8}$$

Furthermore, there exist $z_j \in Z_j$ and $y_j \in Y_j$ with

$$\mathrm{D}_{\mathrm{NC}}(w_j - u_2) = \mathrm{D}\, z_j + y_j \quad \text{on } \Omega_j.$$

Since Y_j is the orthogonal complement of $\mathrm{D}(Z_j)$ in $L^2(\Omega_j;\mathbb{R}^{2\times 2})$, it follows

$$\big\|\mathrm{D}_{\mathrm{NC}}(w_j - u_2)\big\|^2_{L^2(\Omega_j)} = \big\|\mathrm{D}\, z_j\big\|^2_{L^2(\Omega_j)} + \big\|y_j\big\|^2_{L^2(\Omega_j)}. \tag{3.9}$$

The combination of the aforementioned orthogonality with (3.8), $\operatorname{div} z_j = 0$ a.e. in Ω_j, $\operatorname{dev}\sigma_{\mathrm{PS}} = \operatorname{dev}\mathrm{D}_{\mathrm{NC}}\, u_2$ and $f_{\mathcal{T}} + \operatorname{div}\sigma_{\mathrm{PS}} = 0$ yields

$$\begin{aligned}\big\|\mathrm{D}\, z_j\big\|^2_{L^2(\Omega_j)} &= \int_{\Omega_j} \mathrm{D}_{\mathrm{NC}}(w_j - u_2) : \mathrm{D}\, z_j \,\mathrm{d}x = \int_{\Omega_j} \mathrm{D}\, w_j : \mathrm{D}\, z_j \,\mathrm{d}x - \int_{\Omega_j} \mathrm{D}_{\mathrm{NC}}\, u_2 : \mathrm{D}\, z_j \,\mathrm{d}x \\ &= \int_{\Omega_j} f_{\mathcal{T}} \cdot z_j \,\mathrm{d}x - \int_{\Omega_j} \sigma_{\mathrm{PS}} : \mathrm{D}\, z_j \,\mathrm{d}x = \int_{\Omega_j} (f_{\mathcal{T}} + \operatorname{div}\sigma_{\mathrm{PS}}) \cdot z_j \,\mathrm{d}x = 0.\end{aligned} \tag{3.10}$$

Recall from [8, Subsection 3.2, Lemma 2] that, for each $y_j \in Y_j$, there exists some $q_j \in L^2_0(\Omega_j)$ with

$$\int_{\Omega_j} y_j : \mathrm{D}\, \varphi_j \,\mathrm{d}x = \int_{\Omega_j} q_j \operatorname{div}\varphi_j \,\mathrm{d}x \quad \text{for all } \varphi_j \in H^1_0(\Omega_j;\mathbb{R}^2)$$

and

$$c_j \big\|q_j\big\|_{L^2(\Omega_j)} \leqslant \big\|y_j\big\|_{L^2(\Omega_j)}.$$

The combination of this result for the test function $\varphi_j \equiv w_j - v \in H^1_0(\Omega_j;\mathbb{R}^2)$ with the aforementioned orthogonality and a Cauchy inequality result in

$$\begin{aligned}\big\|y_j\big\|^2_{L^2(\Omega_j)} &= \int_{\Omega_j} y_j : \mathrm{D}_{\mathrm{NC}}(w_j - u_2)\,\mathrm{d}x = \int_{\Omega_j} y_j : \mathrm{D}_{\mathrm{NC}}(v - u_2)\,\mathrm{d}x + \int_{\Omega_j} y_j : \mathrm{D}_{\mathrm{NC}}(w_j - v)\,\mathrm{d}x \\ &\leqslant \Big(\big\|\mathrm{D}_{\mathrm{NC}}(v - u_2)\big\|_{L^2(\Omega_j)} + \big\|\operatorname{div}\varphi_j\big\|_{L^2(\Omega_j)}/c_j\Big)\,\big\|y_j\big\|_{L^2(\Omega_j)}.\end{aligned}$$

This, (3.9), (3.10), and $\operatorname{div} w_j = 0$ a.e. in Ω_j imply, for $j = 1, \ldots, J$,

$$\big\|\mathrm{D}_{\mathrm{NC}}(w_j - u_2)\big\|_{L^2(\Omega_j)} = \big\|y_j\big\|_{L^2(\Omega_j)} \leqslant \big\|\mathrm{D}_{\mathrm{NC}}(v - u_2)\big\|_{L^2(\Omega_j)} + \big\|\operatorname{div} v\big\|_{L^2(\Omega_j)}/c_j. \tag{3.11}$$

The functions $w_j, z_j \in H^1_0(\Omega_j;\mathbb{R}^2)$ can be extended by zero to $\widetilde{w}_j, \widetilde{z}_j \in H^1_0(\Omega;\mathbb{R}^2)$ (i.e. $\widetilde{w}_j := w_j$ and $\widetilde{z}_j := z_j$ in Ω_j and $\widetilde{w}_j, \widetilde{z}_j := 0$ in $\Omega\backslash\Omega_j$) and $y_j \in L^2(\Omega_j;\mathbb{R}^{2\times 2})$ can be extended by zero to $\widetilde{y}_j \in L^2(\Omega;\mathbb{R}^{2\times 2})$ (i.e. $\widetilde{y}_j := y_j$ in Ω_j and $\widetilde{y}_j := 0$ in $\Omega\backslash\Omega_j$). Then the sums $\widetilde{z} := \widetilde{z}_1 + \ldots + \widetilde{z}_J$ and $\widetilde{w} := \widetilde{w}_1 + \ldots + \widetilde{w}_J$ belong to Z.

Since $\operatorname{div}\widetilde{w} = 0$ a.e. in Ω, part (a) proves for $\widetilde{w} \in \mathcal{A}$ that

$$\big|\!\big|\!\big|u - u_2\big|\!\big|\!\big|^2_{\mathrm{NC}} \leqslant \operatorname{osc}(f,\mathcal{T})^2/j^2_{1,1} + \big|\!\big|\!\big|\widetilde{w} - u_2\big|\!\big|\!\big|^2_{\mathrm{NC}}.$$

The estimate (3.11) implies

$$\big|\!\big|\!\big|\widetilde{w} - u_2\big|\!\big|\!\big|^2_{\mathrm{NC}} = \sum_{j=1}^{J} \big\|\mathrm{D}_{\mathrm{NC}}(w_j - u_2)\big\|^2_{L^2(\Omega_j)} \leqslant \sum_{j=1}^{J} \Big(\big\|\mathrm{D}_{\mathrm{NC}}(v - u_2)\big\|_{L^2(\Omega_j)} + \big\|\operatorname{div} v\big\|_{L^2(\Omega_j)}/c_j\Big)^2.$$

This concludes the proof of (b). □

4. Proper Interpolation Designs

This section designs functions $v \in \widetilde{\mathcal{A}}$ with the additional prerequisites

$$\int_{\partial\Omega_j} v \cdot \nu_{\Omega_j} \,\mathrm{d}s = 0 \quad \text{for } j = 1, \dots, J \tag{4.1}$$

for Theorem 3.1 (b) by modifications of the designs compared in [13]. All designs satisfy a discrete Dirichlet boundary condition of the set of admissable functions defined by

$$\begin{aligned}
&\mathcal{A}(\mathcal{T}) := \{v \in C(\overline{\Omega}; \mathbb{R}^2) \,:\, v(z) = u_D(z) \text{ for all } z \in \mathcal{N}(\partial\Omega)\} \quad \text{and} \\
&\widetilde{\mathcal{A}}(\mathcal{T}) := \{v \in \mathcal{A}(\mathcal{T}) \,:\, v \text{ satisfies (4.1)}\}.
\end{aligned}$$

These functions violate the exact Dirichlet boundary condition, see Subsection 4.4 for a remedy. Furthermore, $\mathcal{E}(\Gamma) := \{E \in \mathcal{E} \,:\, E \subseteq \Gamma\}$ defines the set of edges along the skeleton $\Gamma := \bigcup_{j=1}^{J} \partial\Omega_j$.

4.1. Piecewise quadratic interpolation.

A nodal averaging of u_2 as in [13] leads to the piecewise quadratic and continuous function $v_{\mathrm{AP2}} \in P_2(\mathcal{T}; \mathbb{R}^2) \cap \widetilde{\mathcal{A}}(\mathcal{T})$, defined via piecewise quadratic interpolation of the values at the nodes $z \in \mathcal{N}$

$$v_{\mathrm{AP2}}(z) := \begin{cases} u_D(z) & \text{for } z \in \mathcal{N}(\partial\Omega), \\ \sum_{T \in \mathcal{T}(z)} u_2|_T(z) \Big/ \big|\mathcal{T}(z)\big| & \text{for } z \in \mathcal{N}(\Omega), \end{cases}$$

and in the midpoints of the edges $E \in \mathcal{E}$ with the two adjacent triangles $\mathcal{T}(\mathrm{mid}(E))$ of $E \in \mathcal{E}(\Omega)$ and the two endpoints $\mathcal{N}(E)$

$$v_{\mathrm{AP2}}(\mathrm{mid}(E)) := \begin{cases} \sum_{T \in \mathcal{T}(\mathrm{mid}(E))} u_2|_T(\mathrm{mid}(E)) \Big/ \big|\mathcal{T}(\mathrm{mid}(E))\big| & \text{for } E \in \mathcal{E}(\Omega) \backslash \mathcal{E}(\Gamma), \\ 3\widehat{u}_{\mathrm{CR}}(\mathrm{mid}(E))/2 - \sum_{z \in \mathcal{N}(E)} v_{\mathrm{AP2}}(z)/4 & \text{for } E \in \mathcal{E}(\Gamma). \end{cases}$$

Let $(\varphi_z \,:\, z \in \mathcal{N} \cup \mathrm{mid}(\mathcal{E}))$ denote the piecewise quadratic and globally continuous basis functions of $P_2(\mathcal{T}) \cap C(\overline{\Omega})$. The definition of v_{AP2} implies

$$\begin{aligned}
&\int_{\partial\Omega_j} v_{\mathrm{AP2}} \cdot \nu \,\mathrm{d}s = \sum_{E \in \mathcal{E}(\partial\Omega_j)} \int_E v_{\mathrm{AP2}} \cdot \nu \,\mathrm{d}s \\
&= \sum_{E \in \mathcal{E}(\partial\Omega_j)} \Big(v_{\mathrm{AP2}}(\mathrm{mid}(E)) \int_E \varphi_{\mathrm{mid}(E)} \,\mathrm{d}s + \sum_{z \in \mathcal{N}(E)} v_{\mathrm{AP2}}(z) \int_E \varphi_z \,\mathrm{d}s \Big) \cdot \nu_{\Omega_j}|_E \\
&= \sum_{E \in \mathcal{E}(\partial\Omega_j)} \big|E\big|/6 \left(4 v_{\mathrm{AP2}}(\mathrm{mid}(E)) + \sum_{z \in \mathcal{N}(E)} v_{\mathrm{AP2}}(z) \right) \cdot \nu_{\Omega_j}|_E \\
&= \sum_{E \in \mathcal{E}(\partial\Omega_j)} \big|E\big| \widehat{u}_{\mathrm{CR}}(\mathrm{mid}(E)) \cdot \nu_{\Omega_j}|_E = \int_{\partial\Omega_j} \widehat{u}_{\mathrm{CR}} \cdot \nu_{\Omega_j} \,\mathrm{d}s = \int_{\Omega_j} \mathrm{div}\, \widehat{u}_{\mathrm{CR}} \,\mathrm{d}x = 0.
\end{aligned}$$

Hence, $v \equiv v_{\mathrm{AP2}}$ satisfies condition (4.1).

4.2. **Minimal piecewise quadratic interpolation.** A global minimization of the guaranteed upper bound from Theorem 3.1 (b) leads to

$$\begin{aligned} v_{\mathrm{MP2}} &\coloneqq \operatorname*{argmin}_{v\in P_2(\mathcal{T};\mathbb{R}^2)\cap\widetilde{\mathcal{A}}(\mathcal{T})} \sum_{j=1}^{J} \Big(\big\| \operatorname{D_{NC}}(v-u_2)\big\|_{L^2(\Omega_j)} + \big\| \operatorname{div} v\big\|_{L^2(\Omega_j)}/c_j \Big)^2 \\ &= \operatorname*{argmin}_{v\in P_2(\mathcal{T};\mathbb{R}^2)\cap\widetilde{\mathcal{A}}(\mathcal{T})} \sum_{j=1}^{J} \min_{0<\mu_j<\infty} \Big((1+\mu_j)\big\| \operatorname{D_{NC}}(v-u_2)\big\|^2_{L^2(\Omega_j)} \\ &\qquad\qquad + (1+1/\mu_j)\big\| \operatorname{div} v\big\|^2_{L^2(\Omega_j)}/c_j^2 \Big) \end{aligned}$$

and is realised by the following algorithm.

Algorithm 4.1 (global minimization)**.** ***Input*** $\widehat{u}_2 \in P_2(\mathcal{T};\mathbb{R}^2), c_1,\dots,c_j,\Omega_1,\dots,\Omega_J$ *and the number of iterations* $K\in\mathbb{N}$.
Initialize $\mu_j \coloneqq 1$ *for* $j=1,\dots,J$.
for $k=1,\dots,K$ ***do***
Compute $v_{\mathrm{MP2}(k)} \coloneqq$

$$\operatorname*{argmin}_{v\in P_2(\mathcal{T};\mathbb{R}^2)\cap\widetilde{\mathcal{A}}(\mathcal{T})} \sum_{j=1}^{J} \Big((1+\mu_j)\big\| \operatorname{D_{NC}}(v-u_2)\big\|^2_{L^2(\Omega_j)} + (1+1/\mu_j)\big\| \operatorname{div} v\big\|^2_{L^2(\Omega_j)}/c_j^2 \Big),$$

$\mu_j \coloneqq \big\| \operatorname{div} v_{\mathrm{MP2}(k)}\big\|_{L^2(\Omega_j)} \Big/ \big(c_j \big\| \operatorname{D_{NC}}(v_{\mathrm{MP2}(k)}-u_2)\big\|_{L^2(\Omega_j)}\big)$ *for* $j=1,\dots,J$. ***od***
Output $v_{\mathrm{MP2}(K)} \in P_2(\mathcal{T};\mathbb{R}^2)\cap\widetilde{\mathcal{A}}(\mathcal{T})$.

The condition (4.1) (involved in $\widetilde{\mathcal{A}}(\mathcal{T})$) may be enforced by Lagrange multipliers $\lambda\in\mathbb{R}^J$. The computation of $v_{\mathrm{MP2}(k)}$ requires a solution of a linear system in each step. In order to reduce the computational costs, we use three iterations of a preconditioned conjugate gradient method for inexact solve and denote the solution with $v_{\mathrm{MP2CG3}(K)}$. The preconditioner is the diagonal of the system matrix named after Jacobi. Note that this solution might not satisfy condition (4.1) exactly. For a remedy, the reader is referred to Subsection 4.5.

Undisplayed numerical experiments show that the values after $K=3$ iterations do not significantly change anymore.

4.3. **Piecewise linear interpolation on red-refinement.** This subsection designs piecewise linear $v_{\mathrm{red}} \in P_1(\mathrm{red}(\mathcal{T});\mathbb{R}^2)\cap\widetilde{\mathcal{A}}(\mathcal{T})$ with respect to the uniform red-refinement $\mathrm{red}(\mathcal{T})$ of triangulation $\mathcal{T}$ [7, 13]. The nodes of $\mathrm{red}(\mathcal{T})$ consists of the nodes $\mathcal{N}$ and the edge midpoints $\mathrm{mid}(\mathcal{E})$ of $\mathcal{T}$. Define $v_{\mathrm{red}} \in P_1(\mathrm{red}(\mathcal{T});\mathbb{R}^2)\cap\widetilde{\mathcal{A}}(\mathcal{T})$ via piecewise linear interpolation of the values, for the node $z\in\mathcal{N}$,

$$v_{\mathrm{red}}(z) \coloneqq \begin{cases} u_D(z) & \text{for } z\in\mathcal{N}(\partial\Omega), \\ v_z & \text{for } z\in\mathcal{N}(\Omega) \end{cases} \tag{4.2}$$

with some particular choice of $v_z\in\mathbb{R}^2$, and in the midpoints of the edges $E\in\mathcal{E}$,

$$v_{\mathrm{red}}(\mathrm{mid}(E)) \coloneqq \begin{cases} \widehat{u}_{\mathrm{CR}}(\mathrm{mid}(E)) & \text{for } E\in\mathcal{E}(\Omega)\backslash\mathcal{E}(\Gamma), \\ 2\widehat{u}_{\mathrm{CR}}(\mathrm{mid}(E)) - \sum_{z\in\mathcal{N}(E)} v_{\mathrm{red}}(z)/2 & \text{for } E\in\mathcal{E}(\Gamma). \end{cases} \tag{4.3}$$

Define $(\varphi_z^{\rm red} : z \in \mathcal{N} \cup {\rm mid}(\mathcal{E}))$ as the nodal basis functions in $P_1({\rm red}(\mathcal{T})) \cap C(\overline{\Omega})$. The definition of $v_{\rm red}$ implies

$$\begin{aligned}
&\int_{\partial\Omega_j} v_{\rm red} \cdot \nu \,{\rm d}s = \sum_{E\in\mathcal{E}(\partial\Omega_j)} \int_E v_{\rm red} \cdot \nu \,{\rm d}s \\
&= \sum_{E\in\mathcal{E}(\partial\Omega_j)} \Big(v_{\rm red}({\rm mid}(E)) \int_E \varphi^{\rm red}_{{\rm mid}(E)} \,{\rm d}s + \sum_{z\in\mathcal{N}(E)} v_{\rm red}(z) \int_E \varphi_z^{\rm red} \,{\rm d}s \Big) \cdot \nu_{\Omega_j}|_E \\
&= \sum_{E\in\mathcal{E}(\partial\Omega_j)} |E|/4 \left(2v_{\rm red}({\rm mid}(E)) + \sum_{z\in\mathcal{N}(E)} v_{\rm red}(z) \right) \cdot \nu_{\Omega_j}|_E \\
&= \sum_{E\in\mathcal{E}(\partial\Omega_j)} |E| \widehat{u}_{\rm CR}({\rm mid}(E)) \cdot \nu_{\Omega_j}|_E = \int_{\partial\Omega_j} \widehat{u}_{\rm CR} \cdot \nu_{\Omega_j} \,{\rm d}s = \int_{\Omega_j} {\rm div}\, \widehat{u}_{\rm CR} \,{\rm d}x = 0.
\end{aligned}$$

Hence, $v \equiv v_{\rm red}$ satisfies condition (4.1).

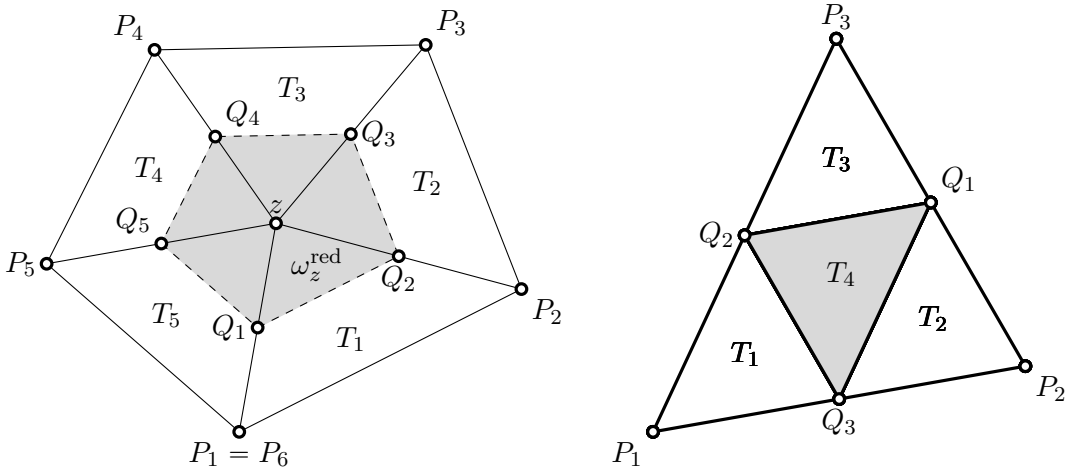

(a) Interior Patch

(b) Central Subtriangle $T_4 = {\rm conv}\{{\rm mid}(\mathcal{E}(T))\}$ in ${\rm red}(T)$ for $T \in \mathcal{T}$.

FIGURE 4.1. Notation for red-refinements.

interpolation $v_{\rm red}$ is fixed on all central subtriangles as T_4 in Figure 4.1(b) and it remains to determine the values v_z at the free nodes $z \in \mathcal{N}(\Omega)$, e.g. by nodal averaging

$$v_z := \sum_{T\in\mathcal{T}(z)} \widehat{u}_{\rm CR}|_T(z) / \big|\mathcal{T}(z)\big| \quad \text{for all } z \in \mathcal{N}(\Omega). \tag{4.4}$$

Algorithm 4.2 below suggests the one-dimensional minimization problem around each node patch $\omega_z^{\rm red}$ with respect to the red-refined triangulation as in Figure 4.1(a) under the side condition of the fixed values at the edge midpoints Q_j of the adjacent edges.

Algorithm 4.2 (patchwise minimization). ***Input*** $\widehat{u}_{\rm CR} \in CR^1(\mathcal{T};\mathbb{R}^2), c_1, \ldots, c_J, \Omega_1, \ldots, \Omega_J$ *and the number of iterations* $K \in \mathbb{N}$.
Initialize $v_{\rm PMred} := \sum_{E\in\mathcal{E}} \widehat{u}_{\rm CR}({\rm mid}(E)) \varphi^{\rm red}_{{\rm mid}(E)}$ *and* $\mu_j := 1$ *for* $j = 1, \ldots, J$.
for $k = 1, \ldots, K$ ***do***
$v_0 := \sum_{E\in\mathcal{E}} v_{\rm PMred}({\rm mid}(E)) \varphi^{\rm red}_{{\rm mid}(E)}$,

$\forall z \in \mathcal{N}(\Omega)$ *compute*

$$v_z \coloneqq \operatorname*{argmin}_{w\in\mathbb{R}^2} \sum_{j=1}^{J} \Big((1+\mu_j) \big\| \mathrm{D_{NC}}(v_0 + w\varphi_z^{\mathrm{red}} - u_2) \big\|^2_{L^2(\omega_z^{\mathrm{red}}\cap\Omega_j)} + (1+1/\mu_j)/c_j^2 \, \big\| \operatorname{div}(v_0 + w\varphi_z^{\mathrm{red}}) \big\|^2_{L^2(\omega_z^{\mathrm{red}}\cap\Omega_j)} \Big),$$

$v_{\mathrm{PMred}} \coloneqq v_0 + \sum_{z\in\mathcal{N}(\Omega)} v_z \varphi_z^{\mathrm{red}}$,
$\forall j = 1, \dots, J$ *compute* $\mu_j \coloneqq \big\| \operatorname{div} v_{\mathrm{PMred}} \big\|_{L^2(\Omega_j)} / \big(c_j \big\| \mathrm{D_{NC}}(v_{\mathrm{PMred}} - u_2) \big\|_{L^2(\Omega_j)} \big)$. ***od***

Output $v_{\mathrm{PMred}} \in P_1(\mathrm{red}(\mathcal{T}); \mathbb{R}^2) \cap \widetilde{\mathcal{A}}(\mathcal{T})$.

Undisplayed numerical experiments show that the values after $K = 3$ iterations do not significantly change anymore.

We distinguish between the optimal version v_{PMred} from Algorithm 4.2, and v_{MAred} with the suboptimal choice v_z from (4.4).

4.4. **Inhomogeneous Dirichlet boundary conditions.** In case of inhomogeneous Dirichlet boundary conditions all designs in Subsections 4.1–4.3 result in some v_{xyz} which does not necessarily belong to $\mathcal{A}$. To heal this shortcoming, a virtual boundary reconstruction $w_D \in H^1(\Omega)$ with $w_D = u_D - v_{\mathrm{xyz}}$ along $\partial\Omega$ as in [21, 7, 13] allows $v \coloneqq v_{\mathrm{xyz}} + w_D \in \mathcal{A}$ and the estimates

$$\begin{aligned} \big\| \mathrm{D_{NC}}(v - u_2) \big\|_{L^2(\Omega_j)} + \big\| \operatorname{div} v \big\|_{L^2(\Omega_j)}/c_j \leqslant{}& \big\| \mathrm{D_{NC}}(v_{\mathrm{xyz}} - u_2) \big\|_{L^2(\Omega_j)} + \big\| \operatorname{div} v_{\mathrm{xyz}} \big\|_{L^2(\Omega_j)}/c_j \\ &+ \big\| \mathrm{D}\, w_D \big\|_{L^2(\Omega_j)} + \big\| \operatorname{div} w_D \big\|_{L^2(\Omega_j)}/c_j. \end{aligned}$$

The divergence and energy norm of w_D can be estimated by [21, Theorem 4.2]

$$\big\| \operatorname{div} w_D \big\|_{L^2(\Omega_j)} \leqslant \sqrt{2} \big\| \mathrm{D}\, w_D \big\|_{L^2(\Omega_j)} \leqslant \sqrt{2}\, C_\gamma \big\| h_{\mathcal{E}}^{3/2} \partial_{\mathcal{E}}^2 (u_D - v_{\mathrm{xyz}})/\partial s^2 \big\|_{L^2(\partial\Omega_j\cap\partial\Omega)}.$$

The construction of w_D ensures $\int_E w_D \,\mathrm{d}s = 0$ for all $E \in \mathcal{E}(\partial\Omega_j)$. Hence, $v \equiv v_{\mathrm{xyz}} + w_D \in \widetilde{\mathcal{A}}(\mathcal{T})$ for any $v_{\mathrm{xyz}} \in \widetilde{\mathcal{A}}(\mathcal{T})$.

For right isosceles triangles, numerical calculations in [7] suggest the constant $C_\gamma = 0.4980$. If $v_{\mathrm{xyz}}|_E$ equals $u_D|_E$ at $\mathcal{N}(E)$ and $\mathrm{mid}(E)$ for all $E \in \mathcal{E}(\partial\Omega)$, w_D can be designed on the red-refined triangulation with halved edge lengths and accordingly reduced constant $C_\gamma = 0.4980/2^{3/2} = 0.1761$.

4.5. **Projection.** This subsection designs a projection operator that projects a given function $v \in P_2(\mathcal{T}; \mathbb{R}^2) \cap \mathcal{A}(\mathcal{T})$ onto a function $\tilde{v} \in P_2(\mathcal{T}; \mathbb{R}^2) \cap \widetilde{\mathcal{A}}(\mathcal{T})$. Consider the constrained minimization problem

$$\min_{w\in P_2(\mathcal{T};\mathbb{R}^2)\cap\widetilde{\mathcal{A}}(\mathcal{T})} \sum_{j=1}^{J} \Big((1+\mu_j) \big\| \mathrm{D}(v-w) \big\|^2_{L^2(\Omega_j)} + (1+1/\mu_j) \big\| \operatorname{div}(v-w) \big\|^2_{L^2(\Omega_j)}/c_j^2 \Big),$$

where $0 < \mu_j < \infty$ is chosen as follows

$$\mu_j \coloneqq \begin{cases} \big\| \operatorname{div} v \big\|_{L^2(\Omega_j)} \Big/ \big(c_j \big\| \mathrm{D_{NC}}(v - u_2) \big\|_{L^2(\Omega_j)} \big) & \text{if } v \in \{v_{\mathrm{MP2}(K)}, v_{\mathrm{MP2CG3}(K)}\}, \\ 1 & \text{otherwise.} \end{cases}$$

For a given enumeration $\mathcal{N} \cup \mathrm{mid}(\mathcal{E}) = \{z_1, \dots, z_M\}$ of the $M \coloneqq \big|\mathcal{N}\big| + \big|\mathcal{E}\big|$ nodes of the triangulation, define the index set of all nodes on the boundary

$$\mathcal{M} \coloneqq \{m \in \{1, \dots, M\} \,:\, z_m \in \partial\Omega\}.$$

Let $(\varphi_z : z \in \mathcal{N} \cup \mathrm{mid}(\mathcal{E}))$ denote the piecewise quadratic and globally continuous basis functions of $P_2(\mathcal{T}) \cap C(\overline{\Omega})$ enumerated according to the nodes of the triangulation, i.e. $\varphi_m := \varphi_{z_m}$ for $m = 1, \dots, M$. Let $x, y \in \mathbb{R}^{2M}$ denote the coefficients of the basis representation of w respectively v,

$$w = \sum_{m=1}^{M} x_m(\varphi_m, 0)^\top + x_{M+m}(0, \varphi_m)^\top \quad \text{and} \quad v = \sum_{m=1}^{M} y_m(\varphi_m, 0)^\top + y_{M+m}(0, \varphi_m)^\top.$$

Then, the minimization problem reads

$$\min_{x \in \mathbb{R}^{2M}} (y - x)^\top A(y - x) \quad \text{s.t. } (x_m, x_{M+m})^\top = u_D(z_m) \text{ for } m \in \mathcal{M} \text{ and } Bx = 0,$$

where $A \in \mathbb{R}^{2M \times 2M}$ is defined via

$$A_{\ell m} := \sum_{j=1}^{J} \Big((1 + \mu_j) \int_{\Omega_j} \mathrm{D}\,\varphi_\ell : \mathrm{D}\,\varphi_m \,\mathrm{d}x + (1 + 1/\mu_j) \int_{\Omega_j} \mathrm{div}\,\varphi_\ell \,\mathrm{div}\,\varphi_m \,\mathrm{d}x / c_j^2 \Big)$$

for $\ell, m = 1, \dots, 2M$ and condition (4.1) is expressed by the rectangular matrix $B \in \mathbb{R}^{J \times 2M}$ with the entries

$$B_{jm} = \int_{\partial\Omega_j} \varphi_m \cdot \nu \,\mathrm{d}s \quad \text{for } j = 1, \dots, J \text{ and } m = 1, \dots, 2M.$$

Introduce J many Lagrangian multipliers $\lambda_1, \dots, \lambda_J$ to ensure the side condition (4.1). Minimizing the Lagrange functional

$$\mathcal{L}(y; x, \lambda) := (y - x)^\top A(y - x) + \lambda^\top Bx$$

leads to the saddle point problem

$$\begin{bmatrix} 2A & B^\top \\ B & 0 \end{bmatrix} \begin{bmatrix} x \\ \lambda \end{bmatrix} = \begin{bmatrix} 2Ay \\ 0 \end{bmatrix}.$$

In order to reduce the computational costs, replace the matrix A by its diagonal $\Lambda := \mathrm{diag}(A)$. Finally, define the desired projection

$$\tilde{v} := \sum_{m=1}^{M} x_m(\varphi_m, 0)^\top + x_{M+m}(0, \varphi_m)^\top \in P_2(\mathcal{T}; \mathbb{R}^2) \cap \widetilde{\mathcal{A}}(\mathcal{T}).$$

5. Numerical Experiments

This section presents some benchmark examples with convergence history plots for the energy error and history plots of efficiency indices for error estimators as a function of numbers of degrees of freedom (ndof). The labels of the graphs refer to the subscripts of the estimator term η_{xyz} as follows, 'AP2' indicates the piecewise quadratic interpolation v_{AP2} and 'MP2' the minimal piecewise quadratic interpolation v_{MP2}, where the following number in brackets indicates the number of iterations K in Algorithm 4.1. 'MAred' and 'PMred' indicate the two different piecewise linear interpolations v_{MAred} and v_{PMred} on the red-refined triangulation. The annotation '(mod)' indicates the modified interpolations according to the side condition (4.1) and '(proj)' indicates the usage of the projection from Subsection 4.5. Both allow for the upper bound from Theorem 3.1 (b).

5.1. **Adaptive algorithm.** The benchmark examples employ the following adaptive algorithm which includes an equivalent modification of the a posteriori error estimator η_{opt} from [3].

Algorithm 5.1 (APSFEM). ***Input*** *Initial regular triangulation $\mathcal{T}_0$ with refinement edges of the polygonal domain Ω into triangles and bulk parameter $0 < \theta \leqslant 1$.*
for *any level $\ell = 0, 1, 2, \dots$* ***do***
Solve (3.1)–(3.2) *with respect to regular triangulation $\mathcal{T}_\ell$ with solution (σ_ℓ, u_ℓ).*
Compute $(\eta_\ell(\mathcal{T}_\ell, T), T \in \mathcal{T}_\ell)$ *with*

$$\eta_{\mathrm{opt}}^2(\mathcal{T}_\ell, T) \coloneqq \mathrm{osc}^2(f, T) + |T| \big\| \operatorname{curl}(\operatorname{dev} \sigma_\ell) \big\|_{L^2(T)}^2 + |T|^{1/2} \sum_{E \in \mathcal{E}(T)} \big\| [\operatorname{dev}(\sigma_\ell) \tau_E]_E \big\|_{L^2(E)}^2$$

and

$$\eta_{\mathrm{opt}}^2(\mathcal{T}_\ell) \coloneqq \sum_{T \in \mathcal{T}} \eta_{\mathrm{opt}}^2(\mathcal{T}_\ell, T).$$

Mark *a subset $\mathcal{M}_\ell$ of $\mathcal{T}_\ell$ of (almost) minimal cardinality $\big|\mathcal{M}_\ell\big|$ with*

$$\theta \eta_\ell^2 \leqslant \eta_\ell^2(\mathcal{M}_\ell) \coloneqq \sum_{T \in \mathcal{M}_\ell} \eta_\ell^2(T).$$

Refine. *Compute the smallest regular refinement $\mathcal{T}_{\ell+1}$ of $\mathcal{T}_\ell$ with $\mathcal{M} \subseteq \mathcal{T}_\ell \backslash \mathcal{T}_{\ell+1}$ by newest vertex bisection.* ***od***
Output *Sequence of discrete solutions $(\sigma_\ell, u_\ell)_{\ell \in \mathbb{N}_0}$ and meshes $(\mathcal{T}_\ell)_{\ell \in \mathbb{N}_0}$.*

Recall from [4], that this algorithm leads to quasi-optimal convergence in the notion of approximation classes.

5.2. **Classical example on L-shaped domain.** The first benchmark problem employs $f(x, y) \equiv 0$ with the exact solution in polar coordinates

$$u(r, \vartheta) = r^\alpha((1+\alpha)\sin(\vartheta) w(\vartheta) + \cos(\vartheta) w'(\vartheta), -(1+\alpha)\cos(\vartheta) w(\vartheta) + \sin(\vartheta) w'(\vartheta))^\top,$$
$$p(r, \vartheta) = -r^{\alpha-1}((1+\alpha)^2 w'(\vartheta) + w'''(\vartheta))/(1-\alpha)$$

on the L-shaped domain $\Omega = (-1, 1)^2 \backslash ((0, 1) \times (-1, 0))$, where

$$w(\vartheta) = 1/(\alpha+1)\sin((\alpha+1)\vartheta)\cos(\alpha\omega) - \cos((\alpha+1)\vartheta) + 1/(\alpha-1)\sin((\alpha-1)\vartheta)\cos(\alpha\omega) + \cos((\alpha-1)\vartheta)$$

for $\alpha = 856399/1572864$ and $\omega = 3\pi/2$ from [22]. The inhomogeneous Dirichlet boundary data are prescribed by the exact solution $u_D(x, y) \coloneqq u(x, y)$ on $\partial\Omega$. The L-shaped domain Ω is partitioned into the three unit squares $\Omega_1 = (-1, 0)^2, \Omega_2 = (-1, 0) \times (0, 1)$ and $\Omega_3 = (0, 1)^2$. Due to theoretical lower bounds by [10, 11], use $0.1601 \leqslant c_0$ and $0.3826 \leqslant c_j$ for $j = 1, 2, 3$.

Figure 5.1 shows the convergence history of the exact energy error for uniform and adaptive mesh refinement by Algorithm 5.1 with $\theta = 0.5$. As known for this example, the convergence rate for the uniform mesh refinement is not optimal, i.e. 0.25 with respect to the number of degrees of freedom (or 0.5 with respect to the mesh width as $h \equiv \mathrm{ndof}^{-1/2}$).

Figure 5.2 shows the efficiency indices for all error estimators for uniform mesh refinement. The main observation is that the efficiency indices for the '(mod)' and '(proj)' error estimators, that allow for the refined upper bounds with the local inf-sup constant from Theorem 3.1 (b), are dramatically improved compared to the error estimators that operate with unmodified designs. In other words, the gain from the change from global to local

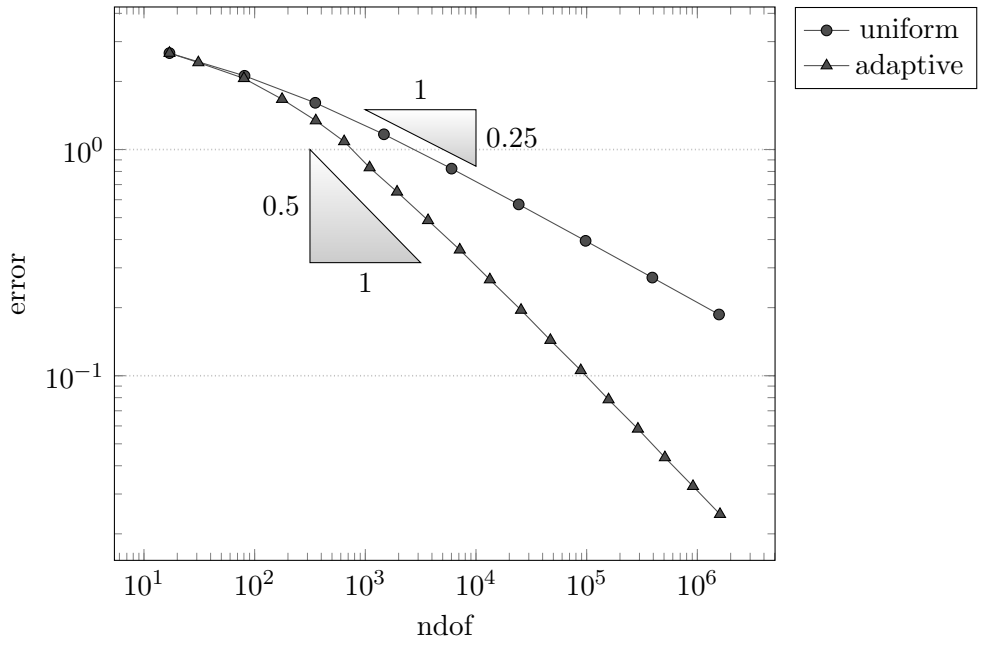

FIGURE 5.1. Convergence history of the energy error for uniform and adaptive mesh refinement for the problem from Subsection 5.2.

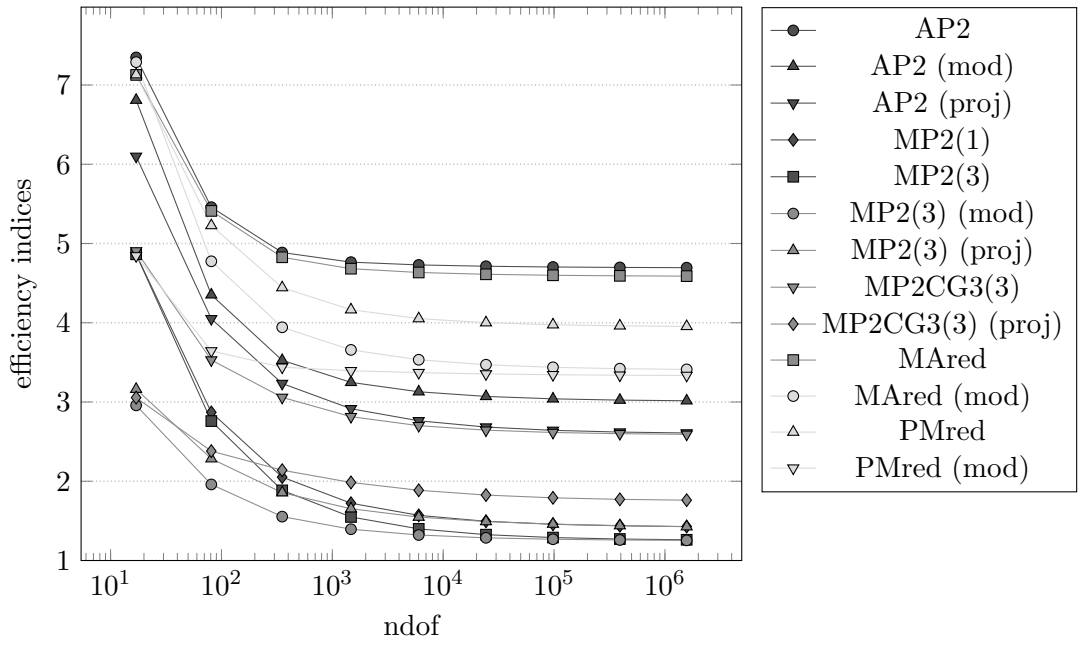

FIGURE 5.2. History of efficiency indices $\eta_{xyz}/|||u-u_h|||$ of various a posteriori error estimators labelled xyz in the figure as functions of the number of unknowns on uniform meshes for the problem from Subsection 5.2.

inf-sup constants is larger than the loss of freedom from the additional constraints in the designs. As an example the efficiency index for η_{AP2} drops from about 4.5 to almost 3.0 for $\eta_{\mathrm{AP2\ (mod)}}$ and the efficiency index for η_{MAred} drops from 4.4 to about 3.5 for $\eta_{\mathrm{MAred\ (mod)}}$. Also the global designs with a truncated minimization benefit from the modifications and

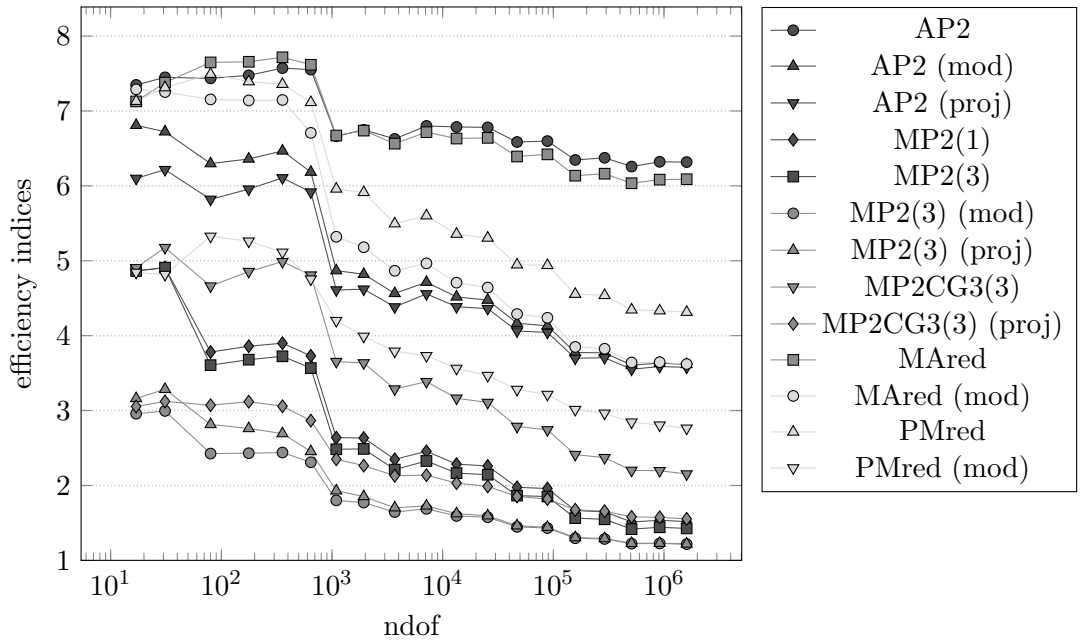

FIGURE 5.3. History of efficiency indices $\eta_{xyz}/|||u-u_h|||$ of various a posteriori error estimators labelled xyz in the figure as functions of the number of unknowns for adaptive mesh refinement for the problem from Subsection 5.2.

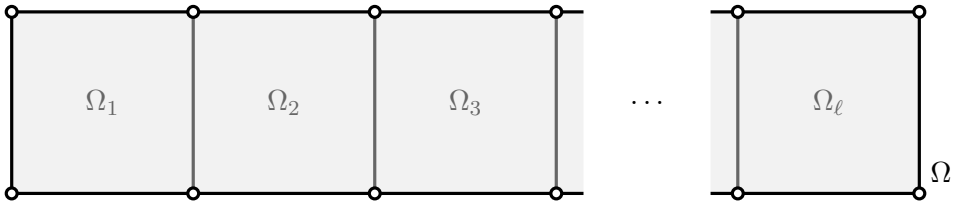

FIGURE 5.4. Subdivision of the domain Ω in the stretched colliding flow example from Subsection 5.3.

the projection. For example, the efficiency index of $\eta_{\mathrm{MP2CG3(3)}}$ of about 2.7 is improved to 1.8 by its modified form $\eta_{\mathrm{MP2CG3(3)\ (proj)}}$. The estimator with the least improvement is $\eta_{\mathrm{MP2(3)}}$ which is due to the fact that its inf-sup constant dependable part of the error estimator is very small at least on fine meshes. The variant $\eta_{\mathrm{MP2(3)\ (proj)}}$ is slighlty less efficient than the variant $\eta_{\mathrm{MP2(3)\ (mod)}}$. Hence, it seems advisable to add the additonal constraint as a side constraint in the minimization problem. However, in case of η_{AP2}, the '(proj)' variant is slightly more efficient than the '(mod)' variant. The efficiency indices for adaptive mesh refinement depicted in Figure 5.3 allow similar conclusions with even more remarkable improvements for the local designs.

5.3. **Colliding flow example on stretched domain.** Given a ratio $\ell \in \mathbb{N}$, let $\Omega := (-1, 2\ell-1) \times (-1, 1)$ denote a stretched domain. The subdivision $\Omega_1, \ldots, \Omega_\ell$ of Ω consists of the ℓ squares with edge length 2 as displayed in Figure 5.4 and lower bounds of the local inf-sup constants $0.3826 \leqslant c_j$ for $j = 1, \ldots, \ell$ from [10, 11]. A computation of a lower bound for the inf-sup constant on star-shaped domains Ω according to [11, Corollary 7 and Proposition 9 i)] yields the lower bounds of c_0 as displayed in Table 1.

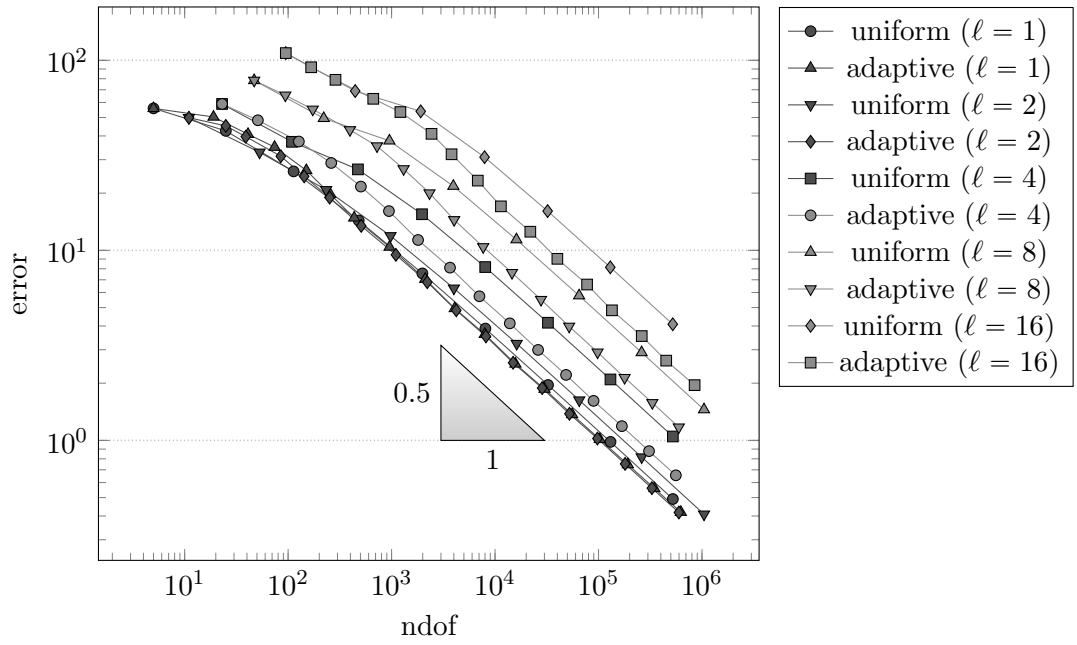

FIGURE 5.5. Convergence history of the exact energy error for uniform and adaptive mesh refinements for the problem from Subsection 5.3.

The second benchmark problem employs $f(x,y) \coloneqq (240(\ell^{-1}(x+1)-1)y^2, 240\ell^{-3}(\ell^{-1}(x+1)-1)^2 y)^\top$ with the exact solution which is derived by transformation of the solution from the colliding flow example to the stretched domain Ω, i.e.,

$$u(x,y) \coloneqq (20(\ell^{-1}(x+1)-1)y^4 - 4(\ell^{-1}(x+1)-1)^5, 20\ell^{-1}(\ell^{-1}(x+1)-1)^4 y - 4\ell^{-1}y^5)^\top,$$
$$p(x,y) \coloneqq -20\ell^{-1}(\ell^{-1}(x+1)-1)^4 - 2\ell^{-1}y^4.$$

Figure 5.5 shows the exact error graphs of the 6 computations with varying parameter $\ell = 1, 2, 4, 8, 16$. The error gets worse for larger domains, but its convergence rates stays optimal.

Table 1 displays the efficiency indices for the computations on a six times red-refined initial triangulation of Ω with $\ell = 1, 2, 4, 8, 16$. In all cases, the error estimators $\eta_{\mathrm{MP2}}, \eta_{\mathrm{MP2\ (mod)}}, \eta_{\mathrm{MP2\ (proj)}}$, and $\eta_{\mathrm{MP2CG3\ (proj)}}$ yield the best results with indices between 1 and 2. When the anisotropy of the domain grows, the global versions of the simple estimators $\eta_{\mathrm{AP2}}, \eta_{\mathrm{MAred}}, \eta_{\mathrm{PMred}}$ get worse. For $\ell = 16$, they reveal extremely poor efficiency indices between 15 and 26 (except for η_{PMred}). However, their local versions exhibit almost no change for increasing ℓ. Their efficiency indices range from 1.8 to 3.7. This is due to the deterioration of the inf-sup-constant c_0 for anisotropic domains, which behaves asymptotically like $\mathcal{O}(\ell^{-1})$ [12, Theorem 3].

5.4. **Backward facing step example.** The third benchmark problem employs $f(x,y) \equiv 0$ on the domain $\Omega = ((-2,8) \times (-1,1)) \backslash ((-2,0) \times (-1,0))$ with Dirichlet boundary data

$$u_D(x,y) = \begin{cases} (-y(y-1)/10, 0) & \text{if } x = -2, \\ (-(y+1)(y-1)/80, 0) & \text{if } x = 8, \\ 0 & \text{otherwise} \end{cases}$$

with a unique, but unknown, weak solution. Therefore the discrete solution on the twice red-refined triangulation is used as a reference solution in the computation of the displayed approximations to the unknown errors. For the refined estimates, the domain Ω is split into

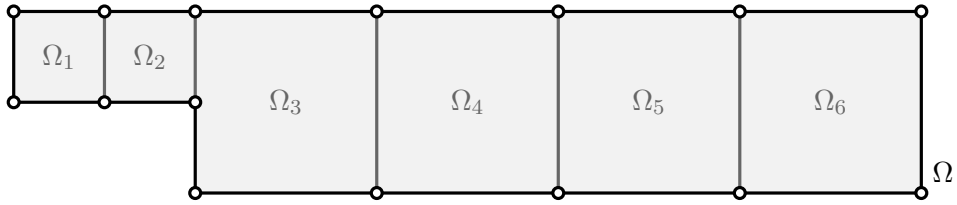

FIGURE 5.6. Subdivision of the domain Ω in the backward facing step example from Subsection 5.4.

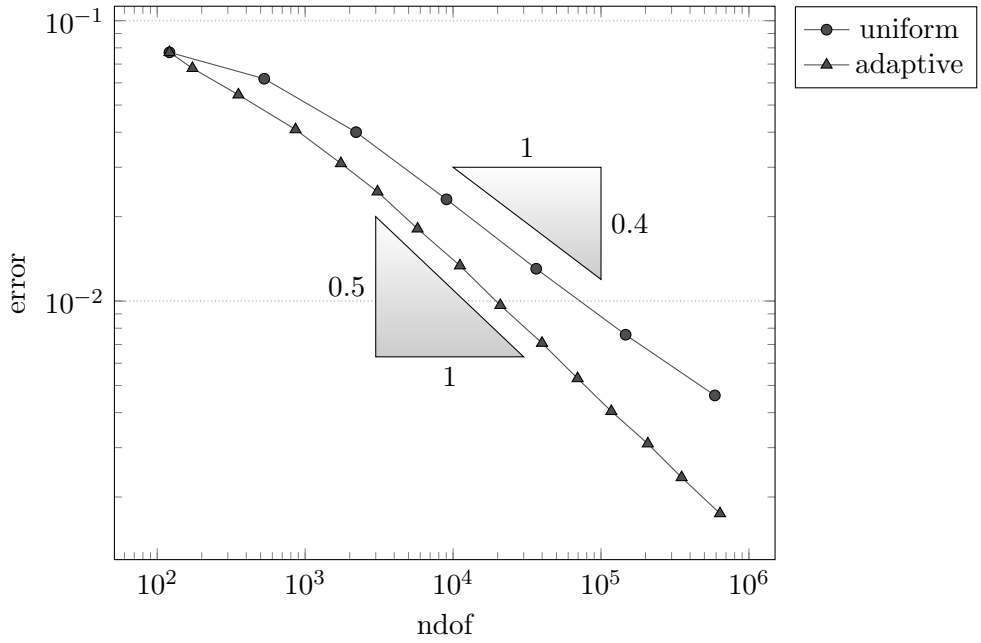

FIGURE 5.7. Convergence history of the energy error with respect to a reference solution on a twice red-refined triangulation for uniform and adaptive mesh refinements for the problem from Subsection 5.4.

six squares as depicted in Figure 5.6 with lower bounds of the local inf-sup constants $0.3826 \leqslant c_j$ for $j = 1, \ldots, 6$ from [10, 11]. The lower bound of the inf-sup constant $0.049814 \leqslant c_0$ in this computation is derived from the formula in [11, Corollary 7]. Up to the authors' knowledge, the assumption in this corollary is not satisfied for Ω. In fact, the true inf-sup constant c_0 might be smaller.

As seen in the previous examples, the adaptive mesh-refinement results in an optimal convergence rate of 0.5 (cf. Figure 5.7).

Figures 5.8 and 5.9 present the efficiency indices for the error estimators from Section 4. The versions with global inf-sup constant exhibit extremely bad efficiency indices in the range of 8 to 22 for η_{AP2} and η_{MAred}. Significantly better, but still worse are the efficiency indices for η_{PMred} of about 8 to 10 for adaptive mesh refinement. These error estimators are most affected by the very small global inf-sup constant of the specific domain Ω. However, the global version of η_{MP2} still yields good efficiency indices close to 1 because the computed test function v_{MP2} is almost divergence free. Its computationally much cheaper modification η_{MP2CG3} is slightly worse with an index of about 3 for adaptive mesh refinement.

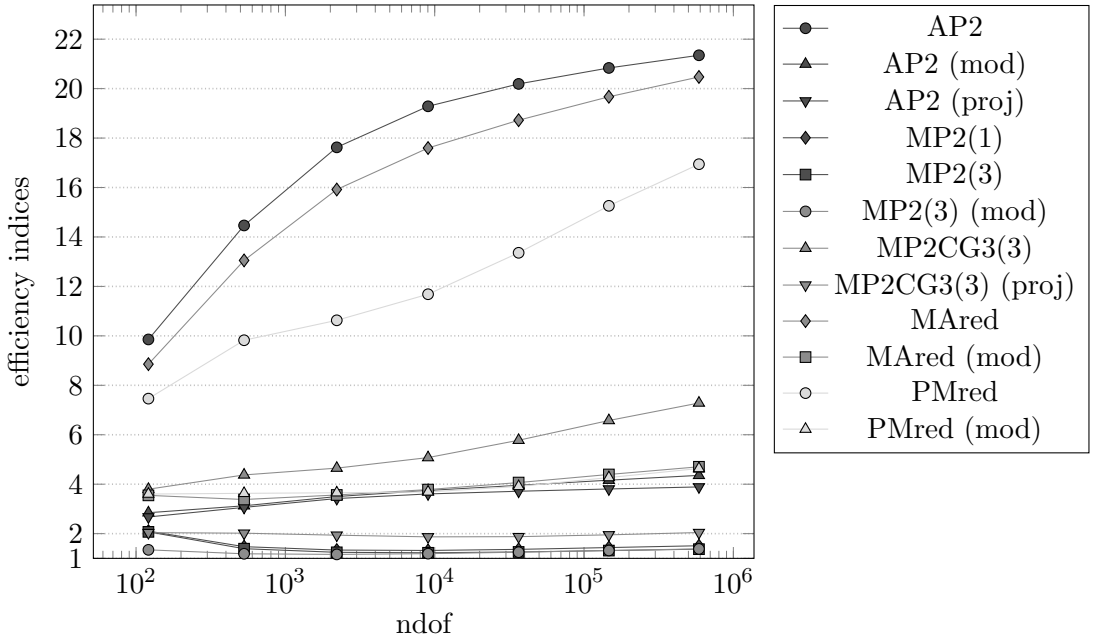

FIGURE 5.8. History of efficiency indices $\eta_{xyz}/|||u-u_h|||$ of various a posteriori error estimators labelled xyz in the figure as functions of the number of unknowns on uniform meshes for the problem from Subsection 5.4.

This benchmark problem once again highlights the exceptional superiority of the proposed designs based on the division of Ω into subdomains and the computation with local inf-sup constants by Theorem 3.1 (b) as suggested by [9]. From the very beginning the estimators with local modification or projection exhibit efficiency indices below 5 in the uniform case and below 4 in the adaptive case. Even the index of the moderate estimator η_{MP2CG3} can be drastically reduced by a factor of at least 2 by using the projected version. It is also remarkable that the computationally cheap but localized upper bounds $\eta_{\mathrm{AP2\ (mod)}}, \eta_{\mathrm{AP2(proj)}}, \eta_{\mathrm{MARed\ (mod)}}$, and $\eta_{\mathrm{PMred\ (mod)}}$ compare favourably well with the global estimator η_{MP2CG3}.

REFERENCES

1. Zhiqiang Cai, Barry Lee, and Ping Wang, *Least-squares methods for incompressible Newtonian fluid flow: linear stationary problems*, SIAM J. Numer. Anal. **42** (2004), no. 2, 843–859 (electronic). MR 2084238 (2005i:65180)
2. Zhiqiang Cai and Yanqiu Wang, *A multigrid method for the pseudostress formulation of Stokes problems*, SIAM J. Sci. Comput. **29** (2007), no. 5, 2078–2095 (electronic). MR 2350022 (2008g:65156)
3. Carsten Carstensen, Dongho Kim, and Eun-Jae Park, *A priori and a posteriori pseudostress-velocity mixed finite element error analysis for the Stokes problem*, SIAM J. Numer. Anal. **49** (2011), no. 6, 2501–2523. MR 2873244
4. Carsten Carstensen, Dietmar Gallistl, and Mira Schedensack, *Quasi-optimal Adaptive Pseudostress Approximation of the Stokes Equations*, SIAM J. Numer. Anal. **51** (2013), no. 3, 1715–1734. MR 3066804
5. Carsten Carstensen and Christian Merdon, *Estimator competition for Poisson problems*, J. Comput. Math. **28 (3)** (2010), 309–330.
6. ———, *Effective postprocessing for equilibration a posteriori error estimators*, Numer. Math. **123** (2013), no. 3, 425–459. MR 3018142
7. ———, *Computational survey on a posteriori error estimators for nonconforming finite element methods for the Poisson problem*, J. Comput. Appl. Math. **249** (2013), 74–94. MR 3037808

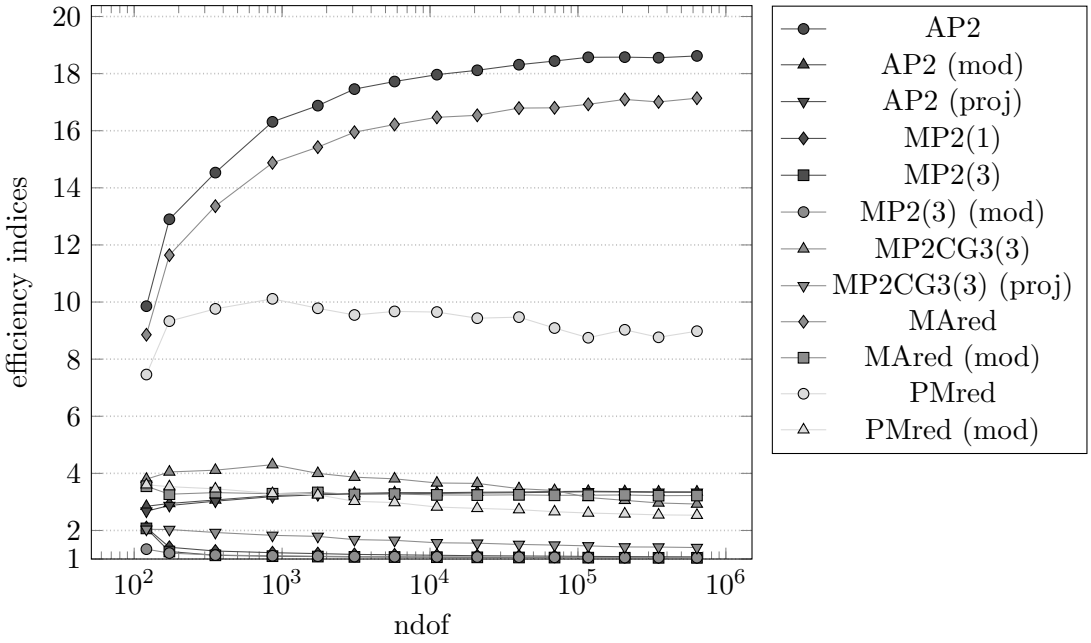

FIGURE 5.9. History of efficiency indices $\eta_{xyz}/|||u-u_h|||$ of various a posteriori error estimators labelled xyz in the figure as functions of the number of unknowns for adaptive mesh refinement for the problem from Subsection 5.4.

8. Mark Ainsworth and Willy Dörfler, *Reliable a posteriori error control for nonconformal finite element approximation of Stokes flow*, Math. Comp. **74** (2005), no. 252, 1599–1619 (electronic).
9. Kwang-Yeon Kim, *Fully computable a posteriori error estimates for the Stokes equation without the global inf-sup constant*, Comput. Math. Appl. **67** (2014), no. 3, 681–691. MR 3149741
10. Gisbert Stoyan, *Towards discrete Velte decompositions and narrow bounds for inf-sup constants*, Comput. Math. Appl. **38** (1999), no. 7-8, 243–261.
11. Monique Dauge, Christine Bernardi, Martin Costabel, and Vivette Girault, *On Friedrichs constant and Horgan-Payne angle for LBB condition*, Twelfth International Conference Zaragoza-Pau on Mathematics, Monogr. Mat. García Galdeano, vol. 39, Prensas Univ. Zaragoza, Zaragoza, 2014, pp. 87–100. MR 3205184
12. M. A. Ol′shanskiĭ and E. V. Chizhonkov, *On the best constant in the inf-sup condition for elongated rectangular domains*, Mat. Zametki **67** (2000), no. 3, 387–396. MR 1779472 (2001g:76020)
13. Carsten Carstensen and Christian Merdon, *Computational Survey on A Posteriori Error Estimators for the Crouzeix–Raviart Nonconforming Finite Element Method for the Stokes Problem*, Comput. Methods Appl. Math. **14** (2014), no. 1, 35–54. MR 3149616
14. Antti Hannukainen, Rolf Stenberg, and Martin Vohralík, *A unified framework for a posteriori error estimation for the Stokes problem*, Numer. Math. **122** (2012), no. 4, 725–769. MR 2995179
15. A. Agouzal, *A posteriori error estimator for nonconforming finite element methods*, Appl. Math. Lett. **7** (1994), no. 5, 61–66.
16. E. Dari, R. Duran, C. Padra, and V. Vampa, *A posteriori error estimators for nonconforming finite element methods*, RAIRO Modél. Math. Anal. Numér. **30** (1996), no. 4, 385–400.
17. S. Bartels, C. Carstensen, and S. Jansche, *A posteriori error estimates for nonconforming finite element methods*, Numer. Math. **92** (2002), 233–256.
18. Carsten Carstensen, Dietmar Gallistl, and Mira Schedensack, *L^2 best-approximation of the elastic stress in the Arnold-Winther FEM*, Preprint 2014-15, Humboldt-Universität zu Berlin, Institut für Mathematik, 2014.
19. Dietrich Braess, *Finite elements - theory, fast solvers, and applications in solid mechanics*, Cambridge University Press, New York, 2007.
20. Richard S. Laugesen and Bartłomiej A. Siudeja, *Minimizing Neumann fundamental tones of triangles: an optimal Poincaré inequality*, J. Differential Equations **249** (2010), no. 1, 118–135. MR 2644129 (2011f:35238)

21. Sören Bartels, Carsten Carstensen, and Georg Dolzmann, *Inhomogeneous Dirichlet conditions in a priori and a posteriori finite element error analysis*, Numer. Math. **99** (2004), no. 1, 1–24.
22. Rüdiger Verfürth, *A posteriori error estimators for the Stokes equations*, Numer. Math. **55** (1989), no. 3, 309–325.

(P. Bringmann) Humboldt-Universität zu Berlin, Unter den Linden 6, 10099 Berlin, Germany.
E-mail address: bringman@math.hu-berlin.de

(C. Carstensen) Humboldt-Universität zu Berlin, Unter den Linden 6, 10099 Berlin, Germany.
E-mail address: cc@math.hu-berlin.de

(C. Merdon) Weierstrass-Institut, Mohrenstr. 39, 10117 Berlin, Germany.
E-mail address: Christian.Merdon@wias-berlin.de

ℓ	ndof	AP2	AP2(mod)	MAred	MAred(mod)	PMred	PMred(mod)
1	32,513	2.1455	2.1781	2.7207	2.7610	2.2257	2.2324
2	65,153	3.0522	2.3069	4.3233	3.1558	2.6221	2.1078
4	130,433	4.8789	2.3780	7.5121	3.3666	2.9824	1.9815
8	260,993	8.5031	2.3906	13.6768	3.4124	3.7073	1.9542
16	522,113	15.7631	2.3901	25.9517	3.4199	5.3061	1.9556

ℓ	MP2(3)	MP2(3)(mod)	MP2CG3(3)	MP2CG3(3)(proj)	c_0
1	1.0377	1.0377	1.2131	1.2131	$3.8268 \cdot 10^{-1}$
2	1.0439	1.0280	1.3304	1.2382	$2.2975 \cdot 10^{-1}$
4	1.0520	1.0174	1.5122	1.2489	$1.2218 \cdot 10^{-1}$
8	1.0612	1.0100	1.8327	1.2481	$6.2137 \cdot 10^{-2}$
16	1.0747	1.0057	2.4606	1.2458	$3.1204 \cdot 10^{-2}$

TABLE 1. Efficiency indices for a collection of estimators for the problem from Subsection 5.3 with different domains for $\ell = 1, 2, 4, 8, 16$. The tables show the results of a computation on the 6 times uniformly red-refined initial triangulation.

List of Figures